nature neuroscience

Behavior-dependent specialization of identified hippocampal interneurons

Damien Lapray[1,2], Balint Lasztoczi[1,2], Michael Lagler[2], Tim James Viney[1], Linda Katona[1], Ornella Valenti[2], Katja Hartwich[1], Zsolt Borhegyi[2], Peter Somogyi[1,2] & Thomas Klausberger[1,2]

A large variety of GABAergic interneurons control information processing in the hippocampal circuits governing the formation of neuronal representations. Whether distinct hippocampal interneuron types contribute differentially to information processing during behavior is not known. We employed a new technique for recording and labeling interneurons and pyramidal cells in drug-free, freely moving rats. Recorded parvalbumin-expressing basket interneurons innervated somata and proximal pyramidal cell dendrites, whereas nitric oxide synthase– and neuropeptide Y–expressing ivy cells provided synaptic and extrasynaptic dendritic modulation. Basket and ivy cells showed distinct spike-timing dynamics, firing at different rates and times during theta and ripple oscillations. Basket, but not ivy, cells changed their firing rates during movement, sleep and quiet wakefulness, suggesting that basket cells coordinate cell assemblies in a behavioral state–contingent manner, whereas persistently firing ivy cells might control network excitability and homeostasis. Different interneuron types provide GABA to specific subcellular domains at defined times and rates, thereby differentially controlling network activity during behavior.

GABAergic interneurons control information processing in cortical circuits as percussionists set the rhythm for a melody or traffic lights regulate the movement of cars through a city. Interneurons generate oscillatory activity[1,2], synchronize the activity of pyramidal cells[3] and set time windows for synaptic integration[4]. A large diversity of interneuronal types is a hallmark of cortical circuits. Different domains of pyramidal cells, such as the soma, axon initial segment, and proximal or distal dendrites[5], are innervated by distinct types of GABAergic interneuron. They also have distinct inputs and membrane properties[6–10] and show different firing patterns during network oscillations induced *in vitro*[11–14] or recorded in anesthetized animals[15], indicating distinct roles for specific interneuron types. However, research on interneurons in drug-free animals that can freely change their behavior has so far been limited to recordings from unidentified interneurons because of technical limitations. In the barrel cortex of head-restrained mice, groups of interneurons with distinct membrane dynamics during different behavioral states have been described[16,17], and in the hippocampus unidentified interneurons or interneurons belonging to heterogeneous groups expressing parvalbumin (PV) and/or somatostatin have been reported[18–21] to fire with different firing patterns during network oscillations. But how do specific types of identified interneurons control the activity of cortical circuits in freely moving animals? Could different types of interneurons make distinct contributions to the information processing during different behaviors? To address these questions, we developed a technique that allowed recordings from unequivocally identified neurons in naturally behaving animals and discovered how two of the most prominent types of hippocampal interneurons contribute to different behavioral states and network operations.

RESULTS

Identification of neurons recorded in freely moving rats

We recorded the activity of PV-expressing basket, ivy and pyramidal cells in the dorsal CA1 area with glass electrodes while drug-free rats were behaving in a recording arena without restraint during movement, natural sleep and quiet wakefulness. Subsequently, recorded cells were juxtacellularly labeled[22] for cell-type identification. We used microdrives for glass electrode placement, and mini-preamplifiers as well as a stable or moveable[23] metal reference electrode in CA1 of the hippocampus or neocortex. A screw in the skull for EEG recordings and tracking devices enabled monitoring of neuronal and behavioral activity (see Online Methods).

PV-expressing basket cells[5] (n = 5) were identified on the basis of their immunoreactivity for PV and their axonal branching in the stratum pyramidale and adjacent layers, where they innervate somata and proximal dendrites of pyramidal and other neurons (**Fig. 1**). For one cell (TV08k), we performed an electron microscopic analysis of 11 randomly sampled synapses and found as synaptic targets the somata (45%), somatic spines (18%) and dendrites (27%) of pyramidal cells, as well as interneuron dendrites (9%). All of the basket cells reported here expressed the Ca^{2+}-binding protein PV and the ErbB4 receptor[24] (**Fig. 1**, **Table 1** and **Supplementary Table 1**). Ivy cells[25,26] (n = 3) had very fine and dense axons in the stratum radiatum

[1]Medical Research Council Anatomical Neuropharmacology Unit, Department of Pharmacology, Oxford University, Oxford, UK. [2]Department of Cognitive Neurobiology, Center for Brain Research, Medical University of Vienna, Vienna, Austria. Correspondence should be addressed to D.L. (damien.lapray@pharm.ox.ac.uk), P.S. (peter.somogyi@pharm.ox.ac.uk) or T.K. (thomas.klausberger@meduniwien.ac.at).

Received 29 May; accepted 28 June; published online 5 August 2012; doi:10.1038/nn.3176

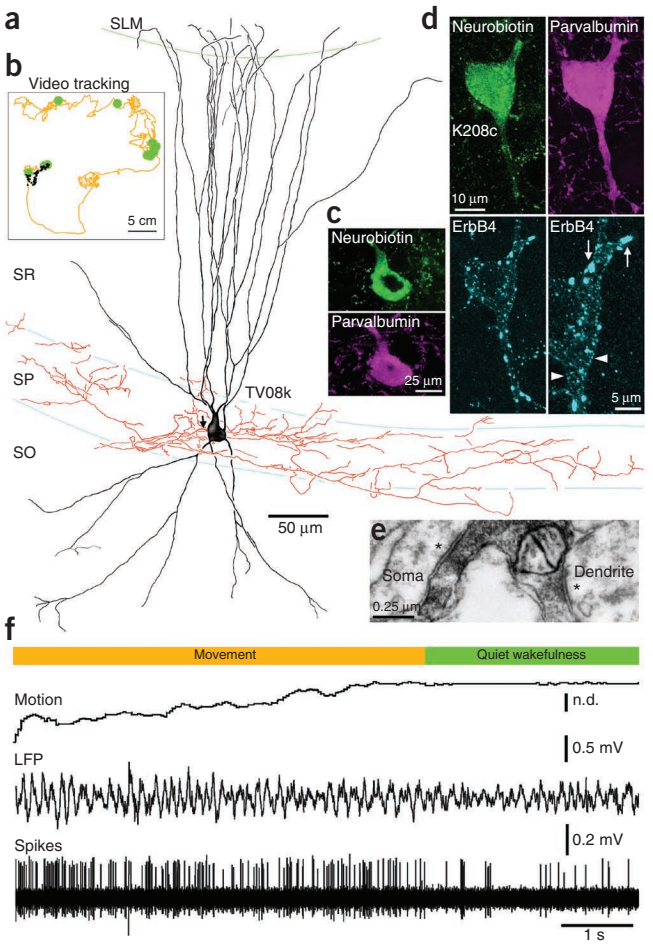

Figure 1 Firing patterns of an identified PV-expressing basket cell during different behavioral states. (**a**) Reconstruction of soma, dendrites (black, complete) and axon (red, one 70-µm-thick section). Arrow indicates the main axon. (**b**) Movements, quiet wakefulness (green circles) and those spikes occurring in the short trace in **f** (black dots) in the recording arena. (**c**) Confocal fluorescence images showing the cell body immunopositive for PV. (**d**) ErbB4 receptor patches (arrows) and continuous membrane labeling (arrowheads) of another recorded basket cell (K208c). (**e**) Electron micrograph of an axonal bouton (from **a**) making type II synapses (asterisks) onto soma and dendrite of pyramidal cells. (**f**) The cell decreased firing at the transition between walking and quiet wakefulness. SLM, stratum lacunosum-moleculare; SR, stratum radiatum; SP, stratum pyramidale; SO, stratum oriens; n.d., normalized distance.

and stratum oriens, which provide synaptic and extrasynaptic GABAergic input to pyramidal cell dendrites. Two of three cells[27] were immunopositive for neuronal nitric oxide synthase (nNOS), and all of the tested cells expressed neuropeptide tyrosine (NPY) and a high level of neurokinin 1 receptor (NK1R), as well as the α1 and δ subunits of $GABA_A$ receptors in the somato-dendritic membrane (**Fig. 2** and **Table 1**). We also analyzed recordings of 14 CA1 pyramidal cells (n = 4 labeled) during different behaviors. Some of these neurons fired as place cells[28–30] during spatial navigation and we tested some of their molecular expression patterns (**Fig. 3** and **Table 1**).

Behavior-specific firing of distinct neurons

For the definition of behavioral states (**Fig. 4** and Online Methods), we used several parameters, including tracking of movements with LED video monitoring and/or an accelerometer. We also used the occurrence of characteristic events such as spindles in the EEG. Pyramidal cells fired with similar mean rates during body movement (2.6 ± 2.3 Hz), slow-wave sleep (1.7 ± 1.4 Hz) and quiet wakefulness (2.2 ± 1.8 Hz) (mean ± s.d., n = 12; P = 0.6 for paired Friedman test; P = 0.3 for repeated-measures ANOVA). However, we observed large variability for different cells and between different periods for the same cell. In contrast, PV-expressing basket cells appeared to change their firing rate dynamically according to the ongoing brain state (**Fig. 5a**). To quantify this observation, we tested individual basket cells and found that four of four tested cells fired at different rates during body movement, slow-wave sleep and quiet wakefulness (P < 0.05, Kruskal Wallis test; the fifth basket cell was not included for this analysis because only one

Table 1 Neurochemical expression profile and firing patterns of recorded cells

Cell group	Cell	Mean theta phase of firing	Mean theta vector length of firing	Median number of spikes per ripple episode	Immunohistochemical test												
					PV	ErbB4	NPY	nNOS	NK1R	GABAARα1	GABAARδ	CCK	Reelin	Somatostatin	SATB2	VIP	Calbindin
PV basket cells	D41n	292.22	0.18	11	+ s	+ s	– s					– s					
	K208c	344.82	0.19	7	+ s,d	+ s,d				+ s,d		– s					
	LK08c	331.87	0.32	4	+ s,a	+ s	– s					nc		nc			
	O83f	232.77	0.2	7	+ d	+ d,a	nc							nc			
	TV08k	239.45	0.2	6	+ s,d	+ d	– s					nc		– s			
Ivy cells	B83k	86.63	0.62	0	– d		+ s	+ s	+ d	+ d	nc						
	D26p	50.22	0.45	0			+ s	+ s	+ d	+ d	+ d		– s			– d	
	ML66a	357.84	0.32	1	– d		+ s	– s	+ d	+ d	+ d						
Pyramidal cells	D19b	215.2	0.29	0													– d
	D30q	224.51	0.31	0													– d
	D35e	149.14	0.09	0								– s			+ s		+ s
	D36w	82.39	0.04	0													– d

+, immunopositive; –, no specific immunoreactivity could be detected in this cell, although other immunopositive cells were observed nearby; nc, not conclusive; s, tested on soma; d, tested on dendrite; a, tested on axon.

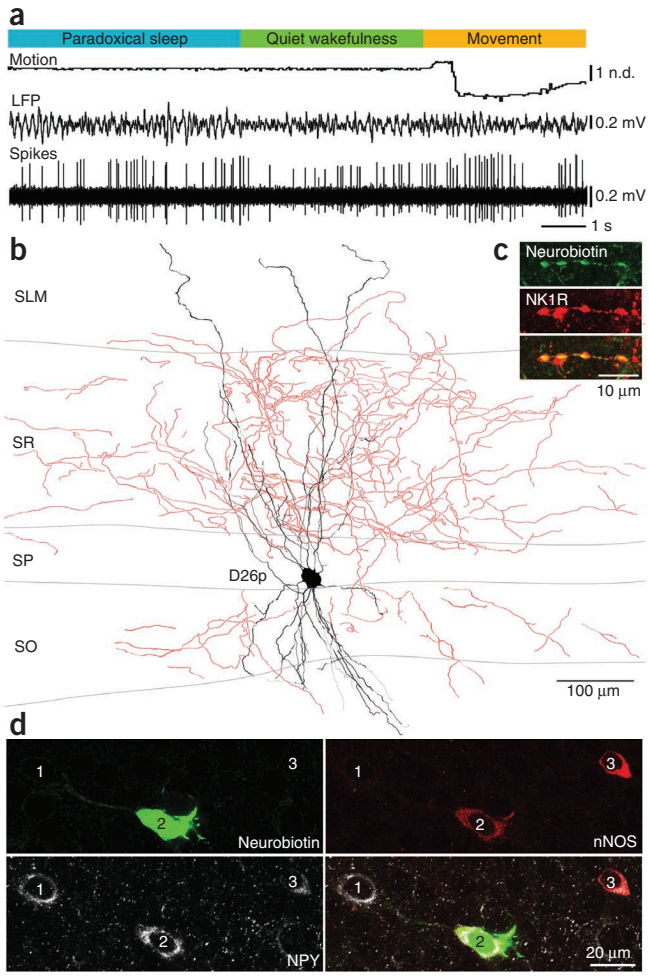

Figure 2 Firing patterns of an identified ivy cell during different behavioral states. (**a**) The cell fired with similar rates during paradoxical sleep, quiet wakefulness and body movement. n.d., normalized distance. (**b**) Reconstruction of the cell (soma and dendrites black, complete; axon red, from one 70-µm-thick section). (**c**) Confocal fluorescence images showing a dendrite of the cell immunopositive for the NK1R. (**d**) The soma (2) is immunopositive for nNOS and NPY; note nearby unrecorded cells (1) immunopositive only for NPY, and a cell (3) positive for both NPY and nNOS.

episode of slow-wave sleep was recorded). Quite the opposite, none of the three ivy cells showed such behavioral state–dependent differences ($P > 0.1$) in firing activity (**Fig. 5b**). As a group (**Fig. 5c**), the mean firing rates of PV-expressing basket cells ($n = 5$) differed ($P = 0.009$ for paired Friedman test, $P = 0.004$ for repeated-measures ANOVA) during slow-wave sleep (31 ± 10 Hz), quiet wakefulness (17 ± 7 Hz) and body movement (24 ± 11 Hz). A *post hoc* Dunn or Bonferroni's test indicated a difference ($P < 0.05$) between firing during slow-wave sleep and quiet wakefulness. In contrast, ivy cells discharged with similar mean rates ($P = 0.9$ for paired Friedman test, $P = 0.9$ for repeated-measures ANOVA; $n = 3$) during body movement (4.0 ± 1.3 Hz), slow-wave sleep (3.8 ± 0.6 Hz) and quiet wakefulness (3.8 ± 1.8 Hz). A mixed-model two-way ANOVA analysis indicated a significant interaction ($P = 0.03$) between the factor cell type and the repeated-measure factor behavioral state ($P < 0.001$ for subject matching shows that the repeated-measures design was effective in controlling for the observed variability; **Fig. 5c**). This suggests that the firing rate changes of the two cell types during distinct behavioral states were different.

Furthermore, we investigated the changes in the interspike intervals of PV-expressing basket and ivy cells during different behavioral states (**Fig. 5d**). Overall, PV-expressing basket cells fired with shorter interspike intervals compared with ivy cells. In addition, PV-expressing basket cells had a higher proportion of interspike intervals at beta and gamma frequency during movement in comparison to slow-wave sleep and quiet wakefulness, but interspike intervals at beta or gamma frequency were hardly observed for ivy cells during movement. These findings indicate that these two types of GABA-releasing interneuron contribute differentially to the organization of the hippocampal network during distinct behavioral states.

Network oscillation–specific firing of distinct neurons

We also measured behavior-dependent network oscillations in the local field potential (LFP) recorded extracellularly in the stratum pyramidale with a metal reference or the glass electrode (**Fig. 6**). Theta oscillations (5–12 Hz) were detected during body movements, paradoxical sleep and, occasionally, quiet wakefulness. Sharp wave–associated ripples (130–230 Hz) were detected during slow-wave sleep and quiet wakefulness. Notably, we also observed short periods with overall low oscillatory activity (**Fig. 6b**). These periods often occurred at transitions between different behavioral states. We defined these periods of overall low oscillatory activity when the power in the theta, beta, slow and fast gamma bands simultaneously dropped below a set threshold (mean – s.d. of the root mean square amplitude in the respective frequency band). After defining the periods of different network oscillations, we analyzed the firing rates of distinct neurons. Pyramidal cells fired during theta oscillations (2.6 ± 2.6 Hz), ripples (6.5 ± 5.4 Hz) and low oscillatory periods (0.8 ± 0.9 Hz) ($P = 0.0001$ for paired Friedman test and $P < 0.05$ for *post hoc* Dunn test for ripples versus theta oscillations and ripples versus low oscillatory periods, $P = 0.0007$ for repeated-measure ANOVA and $P > 0.05$ for *post hoc* Bonferroni's test for ripples versus theta oscillations and ripples versus low oscillatory periods, $n = 14$). PV-expressing basket cells fired differently ($P = 0.008$ for paired Friedman test, $P < 0.0001$ for repeated-measure ANOVA, $n = 5$; **Fig. 6a**) during theta oscillations (21 ± 5 Hz), ripples (122 ± 32 Hz) and low oscillatory periods (6.5 ± 3.4 Hz) ($P < 0.05$ for firing during ripples versus low oscillatory periods with *post hoc* Dunn test, $P < 0.05$ for firing during ripples versus low oscillatory periods and firing during theta oscillations versus low oscillatory periods for repeated-measure ANOVA). In contrast, ivy cells fired with similar rates during the three oscillatory states ($P = 0.4$ for paired Friedman test; $P = 0.6$ for repeated-measure ANOVA; $n = 3$): theta oscillations (2.8 ± 0.8 Hz), ripples (5.2 ± 6.9 Hz) and low oscillatory periods (2.1 ± 1.0 Hz).

Next, we investigated whether PV-expressing basket and ivy cells exhibit different firing patterns during the network oscillations. We observed that PV-expressing basket cells followed the high-frequency ripple oscillations with strong discharges (**Fig. 6c**), in contrast with ivy cells (**Fig. 6d**), which often remained silent during ripples. Individual PV-expressing basket cells fired with 4 to 11 (median) spikes per sharp wave–associated ripple episode. In contrast ($P = 0.03$, Mann Whitney U test), individual ivy cells showed 0 or 1 spike (median) per sharp wave–associated ripple episode (**Fig. 6e**). Notably, ivy cell M66a, which fired with a median of one spike per ripple episode, was nNOS immunonegative and had higher immunoreactivity for δ subunits of $GABA_A$ receptors in the somato-dendritic membrane (**Table 1**). Such highly δ subunit–immunoreactive ivy cells are a minority of the overall population[31].

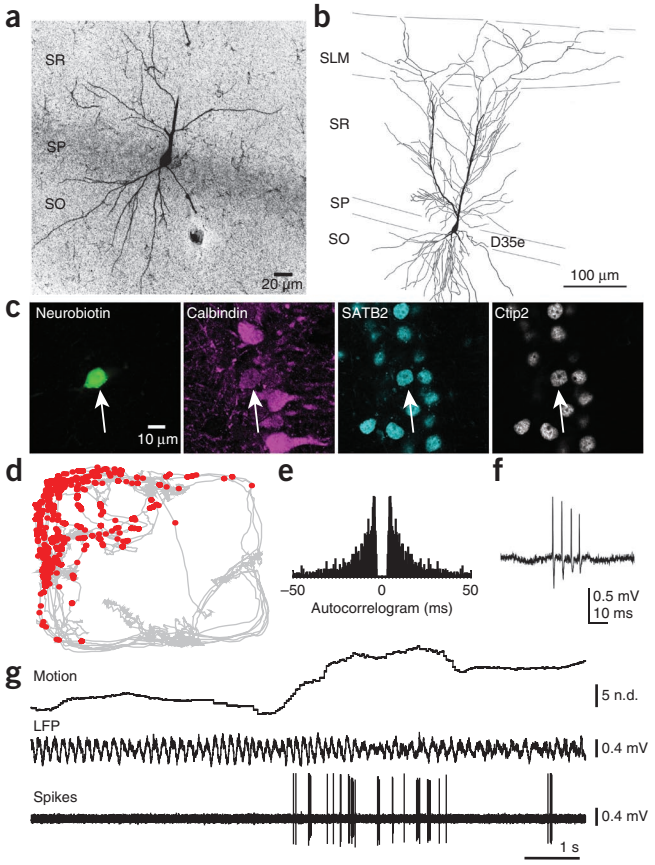

Figure 3 Molecular expression and firing patterns of a place cell. (**a**,**b**) The recorded pyramidal cell was labeled with neurobiotin and visualized by incubation with a streptavidin-conjugated fluorophore (confocal *z* stacks, projection of ten optical sections around the soma, **a**) and its full dendritic tree was reconstructed (six 70-µm-thick sections, **b**). (**c**) This cell is immunopositive for SATB2, Ctip2 and was weakly immunopositive for calbindin. (**d**) The superimposed spikes (filtered >5 cm s^{-1}, red dots) on the path (gray) of the animal indicate a spatial firing preference, the signature of a place cell. (**e**) Autocorrelogram of spike timing. (**f**,**g**) The cell discharged complex spikes (**f**) and showed sparse firing and spatial related activity (**g**).

During theta oscillations, we observed different spike timing of PV-expressing basket and ivy cells. The phase of theta oscillations was always detected in the pyramidal cell layer with either the glass or a metal reference electrode. Basket cells fired at the descending phase of field theta oscillations, on average at 289 ± 48° (0° and 360° mark the trough). In contrast, ivy cells fired at the trough and ascending phase of field theta oscillations, on average at 46 ± 37°. There was no overlap in the mean firing phase of individual basket and ivy cells (**Fig. 6g**), indicating that each cell type modulates pyramidal place cells maximally at different times of the theta cycle. Notably, individual basket cells showed some variability in their mean firing phase during theta oscillations (**Fig. 6g**). The mean firing phase of individual basket cells was similar during theta oscillations occurring at different behavioral states, suggesting that different brain states were not responsible for this variability. However, we observed a relation between the mean firing phase during theta oscillations and the position of the cell in the hippocampus (**Supplementary Fig. 1**). For this analysis, the theta phase was always detected locally from the glass electrode. We observed that PV-expressing basket cells with positions more posterior and lateral in the dorsal CA1 area fired at later phases of the local field theta oscillations (**Fig. 6f**). This observation might reflect a traveling wave of theta oscillations across the hippocampus[32,33].

Ivy cells fired with a similar firing rate across different behavioral states and network oscillations. However, during theta oscillations, we observed some fluctuations in firing rate in the same period (**Fig. 7a**). These fluctuations seemed to be related to the frequency and amplitude of the field theta oscillations. For two ivy and two basket cells, sufficient theta oscillations at different frequencies and amplitudes were recorded to analyze this observation in detail (**Fig. 7b**). The LFP recordings during theta oscillations were subjected to a continuous Morlet wavelet transformation and the instantaneous amplitudes were *z* transformed for each frequency line independently. Amplitude and frequency spectrum averages were plotted against the instantaneous firing rate of the recorded cells in a 200-ms window (see Online Methods). Ivy cells fired sparsely during theta oscillations; thus, in any 200-ms window there were only a few or no spikes (the *x* axis spans a range of only between 0 and 4 spikes per 200 ms). Nevertheless, the firing rate of both ivy cells showed a clear relationship with the frequency and the amplitude of the theta oscillations, that is, an acceleration of theta together with an increase in the cells' firing (**Fig. 7b**). The firing rate of PV-expressing basket cells varied across a much wider dynamic range, but the frequencies of LFP amplitude maxima showed only minor acceleration with increasing spike rate for most of the dynamic range. Although, in general, the firing rate of the

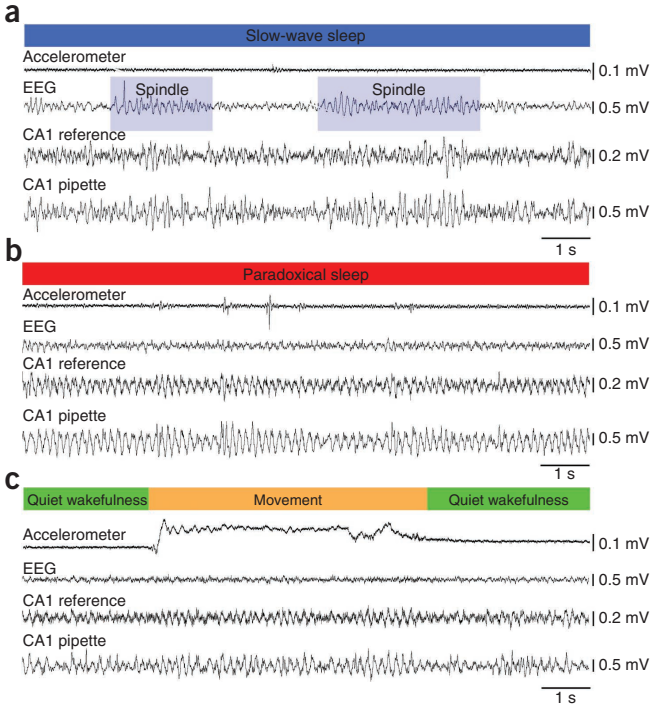

Figure 4 Behavioral state segmentation. (**a**) Slow-wave sleep was characterized by EEG spindles (9–14 Hz, purple rectangles) and large-amplitude slow oscillations (<3 Hz) associated with no movements detected on the accelerometer. (**b**) Predominant theta oscillations on all channels with an absence of movements, except for some fast twitches, defined paradoxical sleep episodes. (**c**) Wakefulness distinguished by a desynchronized low-amplitude EEG was further segmented into quiet wakefulness and movement periods based on activity from the accelerometer.

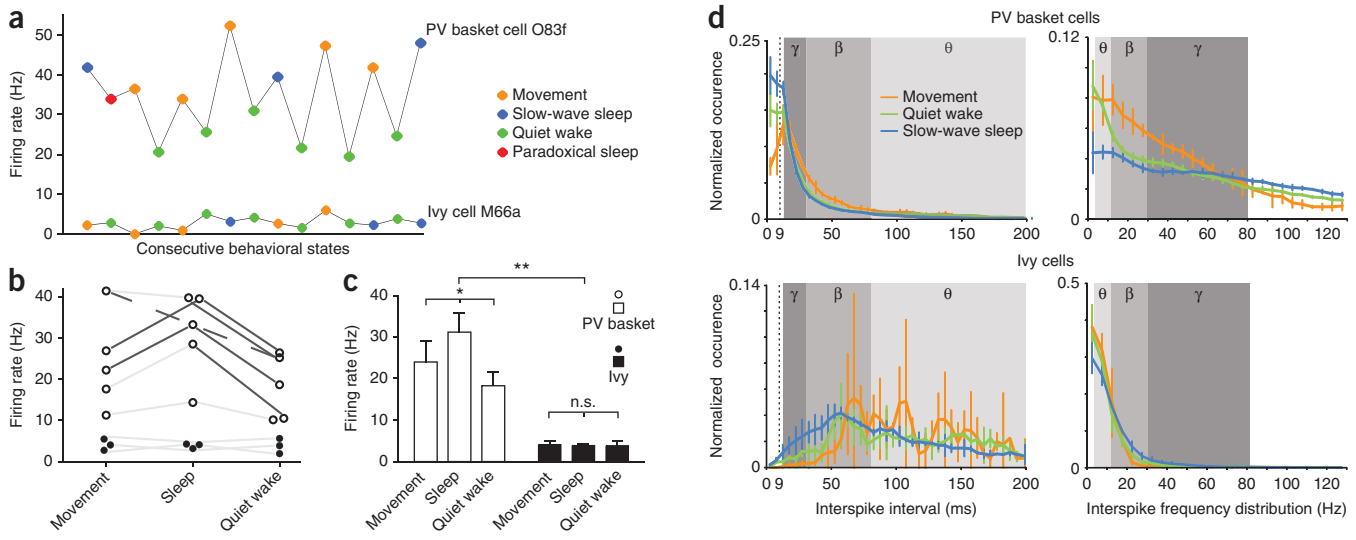

Figure 5 Differential firing of PV-expressing basket and ivy cells during distinct behavioral states. (**a**) Firing rates of a PV-expressing basket and an ivy cell during 15 consecutive behavioral states. (**b**) Individual PV-expressing basket cells (open circles) had different firing rates during movement, slow-wave sleep (excluding paradoxical sleep) and quiet wakefulness, but none of the ivy cells (filled circles) changed firing rates. Lines connect data from individual cells, dark gray lines indicate $P < 0.05$ for *post hoc* Dunn tests after Kruskal Wallis test; dashed gray line indicates significant difference ($P < 0.05$, *post hoc* Dunn test) for a cell between movement and quiet wakefulness. (**c**) The mean firing rates of PV-expressing basket cells (*$P = 0.009$ for paired Friedman test, *$P = 0.004$ for repeated-measures ANOVA, $n = 5$), but not ivy cells (n.s., not significant, $P = 0.9$ for both paired Friedman test and repeated-measures ANOVA, $n = 3$), differed during distinct behavioral states. A mixed-model two-way ANOVA indicated significant differences between the factor cell type (**$P = 0.01$), the repeated-measure factor behavioral state ($P = 0.005$) and the interaction of both factors ($P = 0.03$) with a significant subject matching ($P < 0.001$). Error bars represent mean ± s.e.m. (**d**) Interspike intervals and interspike frequency distributions differed between cell types and behavioral states. Data are presented as mean ± s.e.m. for PV-expressing basket ($n = 5$) and ivy ($n = 3$) cells. For each behavioral state of individual cells, the occurrence was normalized so that the sum of all bins equals 1 for interspike intervals < 350 ms; note the differences in scale between histograms.

PV-expressing basket cells increased together with the amplitude of theta oscillations, an increase in the LFP frequency was not associated with increased firing rates for most of the dynamic range. In summary, both cell types increased their firing with increasing theta amplitude in the LFP. In addition, ivy cells also increased their firing rate with faster frequency theta oscillations (**Fig. 7b**).

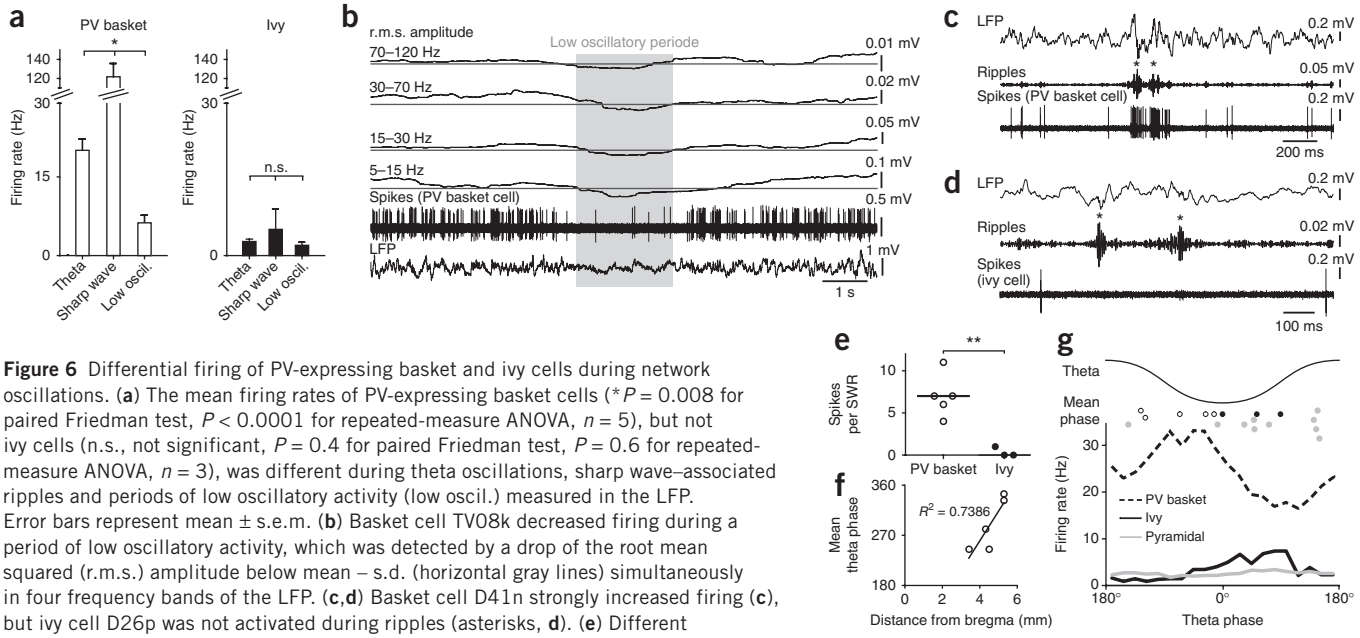

Figure 6 Differential firing of PV-expressing basket and ivy cells during network oscillations. (**a**) The mean firing rates of PV-expressing basket cells (*$P = 0.008$ for paired Friedman test, $P < 0.0001$ for repeated-measure ANOVA, $n = 5$), but not ivy cells (n.s., not significant, $P = 0.4$ for paired Friedman test, $P = 0.6$ for repeated-measure ANOVA, $n = 3$), was different during theta oscillations, sharp wave–associated ripples and periods of low oscillatory activity (low oscil.) measured in the LFP. Error bars represent mean ± s.e.m. (**b**) Basket cell TV08k decreased firing during a period of low oscillatory activity, which was detected by a drop of the root mean squared (r.m.s.) amplitude below mean – s.d. (horizontal gray lines) simultaneously in four frequency bands of the LFP. (**c**,**d**) Basket cell D41n strongly increased firing (**c**), but ivy cell D26p was not activated during ripples (asterisks, **d**). (**e**) Different median numbers of spikes per sharp wave–associated ripple (SWR) episode of PV-expressing basket ($n = 5$) and ivy cells ($n = 3$). **$P = 0.03$, Mann Whitney U test. (**f**) The mean firing phases of PV-expressing basket cells relative to the locally detected theta oscillations were related to the position of the cells in the hippocampus. (**g**) Firing-phase histograms for basket, ivy and pyramidal cells during theta oscillations. Mean firing phases of individual (circles) basket and ivy cells did not overlap.

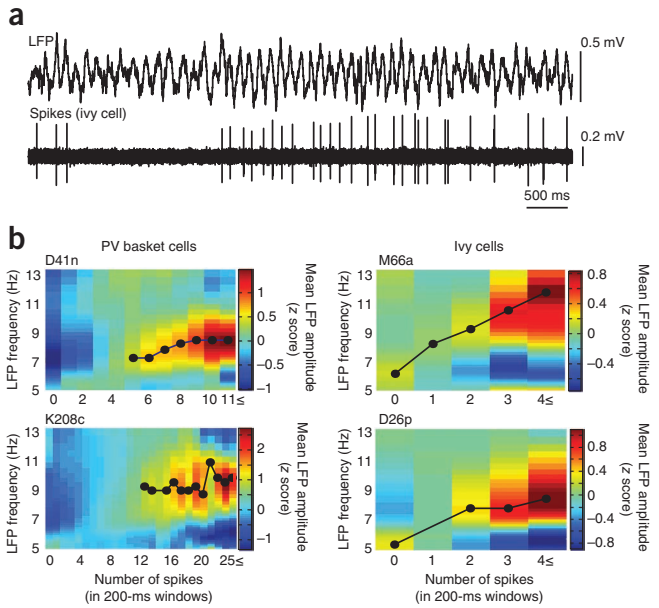

Figure 7 Relationship between frequency and amplitude of theta oscillations and the firing rate of PV-expressing basket and ivy cells. (**a**) Ivy cell D26p increases firing with higher frequency theta oscillations in the LFP. (**b**) Using a Morlet wavelet transformation the average amplitude (*z* transformed, color coded) and frequency of theta oscillations detected in the LFP are plotted as a function of instantaneous firing rate of individual cells (warmest and coldest colors correspond to maxima and minima over the whole plot). Note that the instantaneous rate is given as the number of spikes in a 200-ms window, so 0, 1 and 10 spikes correspond to 0, 5 and 50 Hz, respectively. Black circles indicate detected peaks in LFP amplitude.

DISCUSSION

We found that two distinct types of GABAergic interneurons, PV-expressing basket and ivy cells, the two most numerous GABAergic cell types in the hippocampal pyramidal layer, contribute differentially to behavioral state–dependent neuronal activities and oscillatory network operations in freely moving rats. PV-expressing basket cells are the most studied type of cortical interneuron. So far, an unequivocal recognition of PV-expressing basket cells is only possible by verifying both their molecular expression and axonal arborizations, as PV is also expressed by hippocampal axo-axonic, bistratifed, oriens-lacunosum moleculare and some long-range projection neurons, and because other types of basket cell exist that do not express PV[34]. PV-expressing basket cells are thought to contribute to the generation of network oscillations[2,13,15,35,36] through their highly precise inhibitory control of pyramidal cell output[5,37–39]. They have been predicted to provide a clock-like temporal frame for information coding by pyramidal cells[40]. However, our results indicate that the output of PV-expressing basket cells is dynamically adjusted strongly depending on the ongoing behavior. The basket cells were most active during slow-wave sleep, when sequences of cell assemblies were frequently replayed during sharp wave–associated ripples, which contribute to memory consolidation and transfer to the neocortex[41,42]. Basket cells also provide rhythmic GABAergic input during body movement; they fire at the descending phase of theta oscillations, when pyramidal place cells stop phase-precessing firing and are least active. Notably, we found that, when the animal paused at behavioral state transitions, oscillatory activity could drop in several frequency bands, accompanied by a decrease in the firing of PV-expressing basket cells. This reduced temporal structure may allow network reorganization and the emergence of new cell assemblies.

In contrast with PV-expressing basket cells, which dynamically change their activity during different behaviors, ivy cells fired, on average, with similar rates during slow-wave sleep, body movement, quiet wakefulness and different network oscillations. Ivy cells are the quantitatively most abundant type of GABAergic interneuron in the CA1 area[25]. They provide widespread synaptic and extrasynaptic slow GABAergic input, as well as NPY and nitric oxide to pyramidal cell dendrites and Schaffer collateral and commissural terminals via their exceptionally dense axonal arborizations[25,26] and may mediate the activity-dependent regulation of neurogenesis[43]. The firing patterns identified here are well suited to control homeostasis in the network. We observed that pyramidal cells fired, on average, with similar rates during different behavioral states and they were under constant control via the volume transmission[44] by GABA, NPY and nitric oxide from the dense axonal web of ivy cells. In addition, we observed that ivy cells fired with higher rates when field theta oscillations become faster in frequency and larger in amplitude, reflecting increased network activity and synchrony.

The PV-expressing basket or ivy cells reported here have similar spike timing relative to theta oscillations compared with those recorded under anesthesia[15,25]. This is notable considering that the frequency of theta oscillations was twice as high in drug-free as in anesthetized preparations, and the average firing rates of the neurons were higher in the absence of anesthesia. The preservation of firing phase and the presumed lack of pyramidal cell firing as place or grid cells in the anesthetized rat suggest that the spike timing of interneurons during theta oscillations might be controlled also by external inputs, including those from the medial septum. Furthermore, the firing patterns of each cell type during sharp wave–associated ripples also resembled those recorded under anesthesia. PV-expressing basket cells strongly increased firing, whereas ivy cells did not change their firing rate. Such a preservation of cell type–specific network contribution suggests robust internal network controls across a wide range of input strengths.

Overall, our results show differential contributions of distinct types of interneurons to different behaviors and network operations in freely moving rats, explaining why the temporal dynamics of GABA release is supported by independent sources from specific interneuron types. Because different types of interneuron also provide GABA to different subcellular places, a spatio-temporal matrix of GABAergic inputs dynamically regulates neuronal computations during different behavioral activities.

METHODS

Methods and any associated references are available in the online version of the paper.

Note: Supplementary information is available in the online version of the paper.

ACKNOWLEDGMENTS

The authors thank A. Koroknai for the reconstruction of the dendritic tree of cell D26p, I. Lukacs for the reconstruction of cell TV08k, J. Somogyi for confocal microscopic data acquisition and illustrations, K. Detzner for electron microscopy and immunohistochemistry, R. Hauer and E. Borok for histological processing, T. Sakatani for contributions to microdrive development, B. Micklem for help with the preparation of illustrations, J. O'Neill for help with place cell analysis, Y. Dalezios and G. Dorffner for advice on statistics, and R. Guillery, D. Dupret, M. Capogna, J. Csicsvari and L. Marton for comments on an earlier version of the manuscript. This work was supported in part by grant 242689 of the European Research Council, grant SCIC03 of the Vienna Science and Technology Fund and grant W1205 of the Austrian Science Fund.

AUTHOR CONTRIBUTIONS

All authors contributed to experiments, analysis and manuscript preparation.

COMPETING FINANCIAL INTERESTS
The authors declare no competing financial interests.

Published online at http://www.nature.com/doifinder/10.1038/nn.3176.
Reprints and permissions information is available online at http://www.nature.com/reprints/index.html.

1. Buzsaki, G. *Rhythms of the Brain* (Oxford University Press, New York, 2006).
2. Cardin, J.A. *et al.* Driving fast-spiking cells induces gamma rhythm and controls sensory responses. *Nature* **459**, 663–667 (2009).
3. Cobb, S.R., Buhl, E.H., Halasy, K., Paulsen, O. & Somogyi, P. Synchronization of neuronal activity in hippocampus by individual GABAergic interneurons. *Nature* **378**, 75–78 (1995).
4. Pouille, F. & Scanziani, M. Enforcement of temporal fidelity in pyramidal cells by somatic feed-forward inhibition. *Science* **293**, 1159–1163 (2001).
5. Buhl, E.H., Halasy, K. & Somogyi, P. Diverse sources of hippocampal unitary inhibitory postsynaptic potentials and the number of synaptic release sites. *Nature* **368**, 823–828 (1994).
6. Pawelzik, H., Hughes, D.I. & Thomson, A.M. Physiological and morphological diversity of immunocytochemically defined parvalbumin- and cholecystokinin-positive interneurones in CA1 of the adult rat hippocampus. *J. Comp. Neurol.* **443**, 346–367 (2002).
7. Lamsa, K.P., Heeroma, J.H., Somogyi, P., Rusakov, D.A. & Kullmann, D.M. Anti-Hebbian long-term potentiation in the hippocampal feedback inhibitory circuit. *Science* **315**, 1262–1266 (2007).
8. Fuchs, E.C. *et al.* Recruitment of parvalbumin-positive interneurons determines hippocampal function and associated behavior. *Neuron* **53**, 591–604 (2007).
9. Cossart, R. *et al.* Interneurons targeting similar layers receive synaptic inputs with similar kinetics. *Hippocampus* **16**, 408–420 (2006).
10. Glickfeld, L.L. & Scanziani, M. Distinct timing in the activity of cannabinoid-sensitive and cannabinoid-insensitive basket cells. *Nat. Neurosci.* **9**, 807–815 (2006).
11. Hájos, N. *et al.* Spike timing of distinct types of GABAergic interneuron during hippocampal gamma oscillations *in vitro*. *J. Neurosci.* **24**, 9127–9137 (2004).
12. Gloveli, T. *et al.* Differential involvement of oriens/pyramidale interneurones in hippocampal network oscillations *in vitro*. *J. Physiol. (Lond.)* **562**, 131–147 (2005).
13. Mann, E.O., Suckling, J.M., Hajos, N., Greenfield, S.A. & Paulsen, O. Perisomatic feedback inhibition underlies cholinergically induced fast network oscillations in the rat hippocampus *in vitro*. *Neuron* **45**, 105–117 (2005).
14. Gulyás, A.I. *et al.* Parvalbumin-containing fast-spiking basket cells generate the field potential oscillations induced by cholinergic receptor activation in the hippocampus. *J. Neurosci.* **30**, 15134–15145 (2010).
15. Klausberger, T. *et al.* Brain-state- and cell-type-specific firing of hippocampal interneurons *in vivo*. *Nature* **421**, 844–848 (2003).
16. Gentet, L.J., Avermann, M., Matyas, F., Staiger, J.F. & Petersen, C.C. Membrane potential dynamics of GABAergic neurons in the barrel cortex of behaving mice. *Neuron* **65**, 422–435 (2010).
17. Gentet, L.J. *et al.* Unique functional properties of somatostatin-expressing GABAergic neurons in mouse barrel cortex. *Nat. Neurosci.* **15**, 607–612 (2012).
18. Csicsvari, J., Hirase, H., Czurko, A., Mamiya, A. & Buzsaki, G. Oscillatory coupling of hippocampal pyramidal cells and interneurons in the behaving Rat. *J. Neurosci.* **19**, 274–287 (1999).
19. Maurer, A.P., Cowen, S.L., Burke, S.N., Barnes, C.A. & McNaughton, B.L. Phase precession in hippocampal interneurons showing strong functional coupling to individual pyramidal cells. *J. Neurosci.* **26**, 13485–13492 (2006).
20. Ego–Stengel, V. & Wilson, M.A. Spatial selectivity and theta phase precession in CA1 interneurons. *Hippocampus* **17**, 161–174 (2007).
21. Royer, S. *et al.* Control of timing, rate and bursts of hippocampal place cells by dendritic and somatic inhibition. *Nat. Neurosci.* **15**, 769–775 (2012).
22. Pinault, D. A novel single-cell staining procedure performed *in vivo* under electrophysiological control: morpho-functional features of juxtacellularly labeled thalamic cells and other central neurons with biocytin or Neurobiotin. *J. Neurosci. Methods* **65**, 113–136 (1996).
23. Haiss, F., Butovas, S. & Schwarz, C. A miniaturized chronic microelectrode drive for awake behaving head restrained mice and rats. *J. Neurosci. Methods* **187**, 67–72 (2010).
24. Fazzari, P. *et al.* Control of cortical GABA circuitry development by Nrg1 and ErbB4 signaling. *Nature* **464**, 1376–1380 (2010).
25. Fuentealba, P. *et al.* Ivy cells: a population of nitric oxide–producing, slow-spiking GABAergic neurons and their involvement in hippocampal network activity. *Neuron* **57**, 917–929 (2008).
26. Szabadics, J. & Soltesz, I. Functional specificity of mossy fiber innervation of GABAergic cells in the hippocampus. *J. Neurosci.* **29**, 4239–4251 (2009).
27. Tricoire, L. *et al.* Common origins of hippocampal ivy and nitric oxide synthase–expressing neurogliaform cells. *J. Neurosci.* **30**, 2165–2176 (2010).
28. Epsztein, J., Brecht, M. & Lee, A.K. Intracellular determinants of hippocampal CA1 place and silent cell activity in a novel environment. *Neuron* **70**, 109–120 (2011).
29. Harvey, C.D., Collman, F., Dombeck, D.A. & Tank, D.W. Intracellular dynamics of hippocampal place cells during virtual navigation. *Nature* **461**, 941–946 (2009).
30. O'Keefe, J. Place units in the hippocampus of the freely moving rat. *Exp. Neurol.* **51**, 78–109 (1976).
31. Oláh, S. *et al.* Regulation of cortical microcircuits by unitary GABA-mediated volume transmission. *Nature* **461**, 1278–1281 (2009).
32. Lubenov, E.V. & Siapas, A.G. Hippocampal theta oscillations are travelling waves. *Nature* **459**, 534–539 (2009).
33. Hartwich, K., Pollak, T. & Klausberger, T. Distinct firing patterns of identified basket and dendrite-targeting interneurons in the prefrontal cortex during hippocampal theta and local spindle oscillations. *J. Neurosci.* **29**, 9563–9574 (2009).
34. Klausberger, T. & Somogyi, P. Neuronal diversity and temporal dynamics: the unity of hippocampal circuit operations. *Science* **321**, 53–57 (2008).
35. Ylinen, A. *et al.* Sharp wave–associated high-frequency oscillation (200 Hz) in the intact hippocampus: network and intracellular mechanisms. *J. Neurosci.* **15**, 30–46 (1995).
36. Vida, I., Bartos, M. & Jonas, P. Shunting inhibition improves robustness of gamma oscillations in hippocampal interneuron networks by homogenizing firing rates. *Neuron* **49**, 107–117 (2006).
37. Hu, H., Martina, M. & Jonas, P. Dendritic mechanisms underlying rapid synaptic activation of fast-spiking hippocampal interneurons. *Science* **327**, 52–58 (2010).
38. Losonczy, A., Zemelman, B., Vaziri, A. & Magee, J. Network mechanisms of theta related neuronal activity in hippocampal CA1 pyramidal neurons. *Nat. Neurosci.* **13**, 967–972 (2010).
39. Lovett–Barron, M. Regulation of neuronal input transformations by tunable dendritic inhibition. *Nat. Neurosci.* **15**, 423–430 (2012).
40. Freund, T.F. & Buzsaki, G. Interneurons of the hippocampus. *Hippocampus* **6**, 347–470 (1996).
41. Foster, D.J. & Wilson, M.A. Reverse replay of behavioral sequences in hippocampal place cells during the awake state. *Nature* **440**, 680–683 (2006).
42. Diba, K. & Buzsaki, G. Forward and reverse hippocampal place-cell sequences during ripples. *Nat. Neurosci.* **10**, 1241–1242 (2007).
43. Markwardt, S.J., Dieni, C.V., Wadiche, J.I. & Overstreet-Wadiche, L. Ivy/neurogliaform interneurons coordinate activity in the neurogenic niche. *Nat. Neurosci.* **14**, 1407–1409 (2011).
44. Vizi, E.S. Role of high-affinity receptors and membrane transporters in nonsynaptic communication and drug action in the central nervous system. *Pharm. Rev.* **52**, 63–89 (2000).

ONLINE METHODS

Subjects and housing conditions. All procedures involving animals were performed according to methods approved by the UK Home Office and The Animals (Scientific Procedures) Act (1986) and were approved by the Institutional Animal Care and Use Committees of the University of Oxford and of the Medical University Vienna. Twenty Sprague-Dawley rats (300–550 g) were used in this study. On arrival, animals were housed in groups of 2–4 per cage in Oxford (16 rats, 19–21 °C, 55% humidity, reverse light/dark cycle, lights on from 20:00 to 8:00) or Vienna (4 rats, diurnal cycle, lights on from 6:00 to 18:00). Rats were housed individually 1–7 d before the protocol started with *ad libitum* access to food pellets and water. In addition, chocolate chips were provided to habituate three of the rats to a reward provided during some experimental recordings.

Headstage implantation. Rats were anesthetized with isoflurane (IsoFlo, Abbott) with supplemental intraperitoneal administration of Fentanyl-Janssen (4 µl per 100 g, Janssen-Cilag) in three rats and mounted in a stereotaxic frame (Kopf Instruments). Body temperature was maintained at 37 ± 0.5 °C with a heating pad and breathing was monitored. The skull was exposed and cleaned. Five stainless steel screws were attached to the bone. One was placed above the right prefrontal cortex for EEG recordings (4 mm anterior and 2 mm lateral from bregma); another screw above the cerebellum served as ground/reference. A cylindrical holder for the microdrive was positioned above the left parietal cortex, and EEG and ground screws were connected to a main connector placed above the frontal part of the skull. The whole headstage was embedded in dental acrylic (Refobacin bone cement R, Biomet) except for the region overlying the right hippocampus. The edges of the construction were covered with a smooth layer of blue light–sensitive cement (Tetric EvoFlow, Ivoclar Vivadent). All of the rats were given analgesic treatments (subcutaneous injection of 0.05 ml Rimadyl (Pfizer) or Dipidolor (Janssen-Cilag)), 2 ml per 125 ml of drinking water provided for 48 h after surgery) and some were also given antibiotics (intraperitoneal injection of 0.1 ml 2.5% Baytril (wt/vol), Bayer Vital). Animals were allowed at least three recovery days after headstage implantation. Three rats were food restricted to reach ~85% initial weight before recording started.

Craniotomy and duratomy. After the recovery period, animals were anesthetized with isoflurane and mounted in a stereotaxic frame. Craniotomy and duratomy were performed above the right hippocampus. In between these two procedures, 0.1 mg ml^{-1} of Mitomycin C was applied on the dura mater for 10 min to reduce growth tissue on subsequent days. A single wire (50 µm tungsten, California Fine Wire) was placed in the hippocampus or cortex and either fixed on the skull or mounted on a miniature drive[23]. The cortical surface was protected by a layer of silicone (Kwik-Sil, World Precision Instruments).

Juxtacellular recording and labeling in freely moving rats. The animals were anesthetized 1–10 d after duratomy with isoflurane and mounted in a stereotaxic frame with the ear bars attached directly to the headstage as support. A glass electrode, containing 1.5 or 3% neurobiotin (wt/vol) in 0.5 M NaCl, mounted on a custom-made hydraulic (Narishige) or piezoelectric[45] (Kleindiek Nanotechnik) microdrive, was inserted into the cortex. A miniature pre-amplifier (ELC mini-preamplifier, NPI Electronic) and two LED arrays were connected. In six rats an accelerometer (Supertech International) detected head movements. The cortical surface was protected with wax and the animals were placed in the recording arena (length/width/height: Oxford, 50/50/30 cm; Vienna, 40/60/30 cm). Animals recovered in 5–10 min from anesthesia as reported previously[46], but recording from hippocampal neurons started more than 1 h after recovery from anesthesia (109.4 ± 55.1 min; only two pyramidal cells were recorded before 1 h, after 25 and 50 min, respectively; neither was labeled). Recordings occurred during day time in a room with partially obscured windows (Vienna) or in a darkened room with ambient light (Oxford, mesopic conditions). None of the rats were exposed to the arena before the first recording. After recording, the electrode was advanced toward the recorded neuron for juxtacellular labeling with neurobiotin[22]. Cells were recorded on days 1–12 after duratomy (average 4.6 ± 4.28 d). At the end of the session, the animal was remounted in the stereotaxic frame under isoflurane anesthesia. Recording devices were removed. After successful juxtacellular labeling, the animal was anesthetized and perfusion fixed (see below). If no cell was labeled, the cortex was covered with silicone, the animal was put in its home cage and the procedure was repeated on following days.

Data acquisition. Signals were amplified 1,000× (BF-48DGX and DPA-2FS signal conditioners, NPI Electronic) and digitized at 20 kHz (Power1401 A/D board, Cambridge Electronic Design). Wide-band signals (0.3 Hz to 10 kHz) were acquired in parallel with online filtered single units (0.8–5 kHz) and LFP (0.3–500 Hz) components from the glass electrode. Signals from the hippocampal/cortical electrode and the EEG screw were filtered online at 0.3 Hz to10 kHz. Hum-bugs (Digitimer) were used to remove 50-Hz noise without phase shift. Data from the accelerometer were captured at 1 or 20 kHz from three axes. Signals and video were acquired using Spike2 software (version 7.01, Cambridge Electronics Design) on a personal computer. LED arrays were tracked using a second video camera (Sony, 25 frames per s) and synchronized with the electrophysiological recordings (courtesy of K. Allen).

Immunohistochemical analysis. Cardiac perfusion with saline 1–4 h after cell labeling was followed by ~20 min fixation (4% paraformaldehyde (wt/vol), 15% saturated picric acid (vol/vol) and 0.05% glutaraldehyde (vol/vol) in 0.1 M phosphate buffer at pH ~7.2). Tissue preparation and analysis for light, immunofluorescence[47] (primary antibodies are listed in **Supplementary Table 1**) and electron microscopy[25] was performed as described previously. Two-dimensional reconstructions were made using a drawing tube with a 63× oil-immersion objective.

Analysis of network oscillations. Analysis of network oscillations was performed as described previously[15,47,48], with adjustments for different oscillatory frequencies in drug-free rats. Data processing was done with Spike2 or MATLAB (including the Wavelet Toolbox, version 7.9-R2009b, MathWorks). Periods when the glass electrode might have influenced the firing of the cell were excluded.

The detection of sharp-wave/ripple events and the calculation of discharge frequencies were achieved as described previously[47]. The field potential was filtered between 130 and 230 Hz (Spike2 FIR filter) and the r.m.s. power integrated in a 10-ms sliding window. Peaks of at least 5 s.d. above the mean were considered. All events were validated individually.

The detection of theta epochs were performed as described previously[47]. The theta (5–12 Hz) to delta (2–4 Hz) frequency power ratio was calculated in a 2-s window. A ratio greater than 4 in one window defined a putative theta period. The exact beginning and end points were adjusted manually. Using slightly different detection criteria[49] resulted in the definition of similar theta epochs.

For the detection of low oscillatory periods, the r.m.s. amplitude was calculated in 2-s sliding windows for 5–15, 15–30, 30–70 and 70–120 Hz. A period was accepted when the r.m.s. was below threshold (mean – s.d.) for all four bands simultaneously and for at least 0.3 s. Boundaries were set when the second frequency band dropped below the threshold (start) and the third frequency band reached the threshold (end).

Recordings of the LFP were down-sampled to 1,000 Hz and subjected to a continuous complex-wavelet transformation (Morlet wavelet, wavelet parameters of 1 and 1.5, 38 logarithmically equidistant scales between 5 and 13 Hz). The wavelet transforms were cropped for theta periods (see above), and the modulus (instantaneous amplitude) values were extracted and z transformed for each scale (frequency line) independently. The amplitude spectra corresponding to individual samples were averaged according to the instantaneous spike rate. Instantaneous rate was binned from 0 to n, with increments of 1, where the cumulative number of samples falling into bins from 0 to n included at least 99.9% of all samples (any samples with instantaneous rates above n were added to the bin n).

Definition of behavioral states. Vigilance states were scored manually. Wakefulness was characterized by desynchronized low-amplitude EEG signals lacking spindle oscillations and further segmented into quiet wakefulness (363 episodes, 12.04 s on average ranging from 0.3–110 s) and movement (351 episodes, 7.84 s on average ranging from 0.34–165 s) depending on movement detection (**Fig. 4**). Slow-wave sleep (105 episodes, 38.7 s on average ranging from 6.4–269 s) was defined as the state with high-voltage, slow delta waves (<3 Hz) associated with spindle oscillations (9–14 Hz) and absence of motor activity. Paradoxical sleep (ten episodes, 78.6 s on average ranging from 5–250 s) epochs, always occurring after slow-wave sleep, were defined by a predominant and regular EEG theta rhythm (5–12 Hz) and, despite no movements, the presence of phasic movement twitches. A transition state from slow-wave sleep to paradoxical sleep was identified when spindles and dominant theta oscillation, on EEG and CA1 LFP, respectively, were simultaneously recorded for several seconds.

doi:10.1038/nn.3176

Statistical analysis. Statistical analysis was performed with GraphPad Prism5, MATLAB and the Circular Statistics Toolbox[50]. Comparisons of firing rates were carried out with nonparametric tests, with the exception of the two-way ANOVA, for which an appropriate nonparametric equivalent is not available. For comparisons of paired data within cell types, in addition to the nonparametric Friedman test, a putatively more powerful repeated-measure ANOVA was also performed and results for both tests are reported.

A mixed-model two-way ANOVA was only considered if for subject matching $P < 0.05$ indicated an effective controlling for data variability (GraphPad Prism5). To further test whether the significant interaction observed for data shown in **Figure 5c** was caused only by the different overall firing rates of the two cell types, the average firing rate of the respective cell type was subtracted from all observed firing rate values. The mixed-model two-way ANOVA on this transformed data resulted in a significant interaction of the factor cell type and the repeated-measure factor behavioral state ($P = 0.01$). In another test, all firing rates of ivy cells were multiplied by 4.75 to achieve a simulated match in baseline firing with PV basket cells (same mean firing rate during quiet wakefulness). Also in this transformed data, the mixed-model two-way ANOVA resulted in a significant interaction of the two factors ($P < 0.05$).

We tested the robustness of the observation of similar firing rates of ivy cells ($n = 3$) during different behaviors (**Fig. 5**) or network oscillations (**Fig. 6**). First, we checked whether the test was powerful enough to detect possible differences with $n = 3$. We repeatedly selected three cells from the five PV-expressing basket cells. Ten of ten possible data combinations for network oscillations and seven of ten possible data combinations for behavioral states still showed significant differences for PV-expressing basket cells ($P < 0.05$, repeated-measure ANOVA, $n = 3$), indicating that significant changes in firing rate could be observed with $n = 3$. In another test, we duplicated the observed data for ivy cells (increase of n with low variance), and their firing rate changes remained nonsignificant ($P > 0.25$, repeated-measure ANOVA, $n = 6$). In a different control test, the observed data were supplemented with two values generated randomly within the mean ± s.d. range of the respective data set (increase of n with large variance) and again the firing rate changes of ivy cells remained nonsignificant in all of ten randomly generated data sets ($P > 0.12$, repeated-measure ANOVA, $n = 5$). These tests based on simulated data, taken together with tests on individual ivy cells (**Fig. 5b**) and the two-way ANOVA (**Fig. 5c**), support the observation of similar firing rates of ivy cells across different behavioral states.

45. Lee, A.K., Manns, I.D., Sakmann, B. & Brecht, M. Whole-cell recordings in freely moving rats. *Neuron* **51**, 399–407 (2006).
46. Hacker, S.O., White, C.E. & Black, I.H. A comparison of target-controlled infusion versus volatile inhalant anesthesia for heart rate, respiratory rate, and recovery time in a rat model. *Contemp. Top. Lab. Anim. Sci.* **44**, 7–12 (2005).
47. Lasztóczi, B., Tukker, J.J., Somogyi, P. & Klausberger, T. Terminal field and firing selectivity of cholecystokinin-expressing interneurons in the hippocampal CA3 area. *J. Neurosci.* **31**, 18073–18093 (2011).
48. Klausberger, T. *et al.* Complementary roles of cholecystokinin- and parvalbumin-expressing GABAergic neurons in hippocampal network oscillations. *J. Neurosci.* **25**, 9782–9793 (2005).
49. Louie, K. & Wilson, M.A. Temporally structured replay of awake hippocampal ensemble activity during rapid eye movement sleep. *Neuron* **29**, 145–156 (2001).
50. Berens, P. CircStat: a MATLAB toolbox for circular statistics. *J. Stat. Softw.* **31**, 1–21 (2009).

Behavior-dependent specialization of identified hippocampal interneurons

Damien Lapray, Balint Lasztoczi, Michael Lagler, Tim James Viney, Linda Katona, Ornella Valenti, Katja Hartwich, Zsolt Borhegyi, Peter Somogyi, Thomas Klausberger

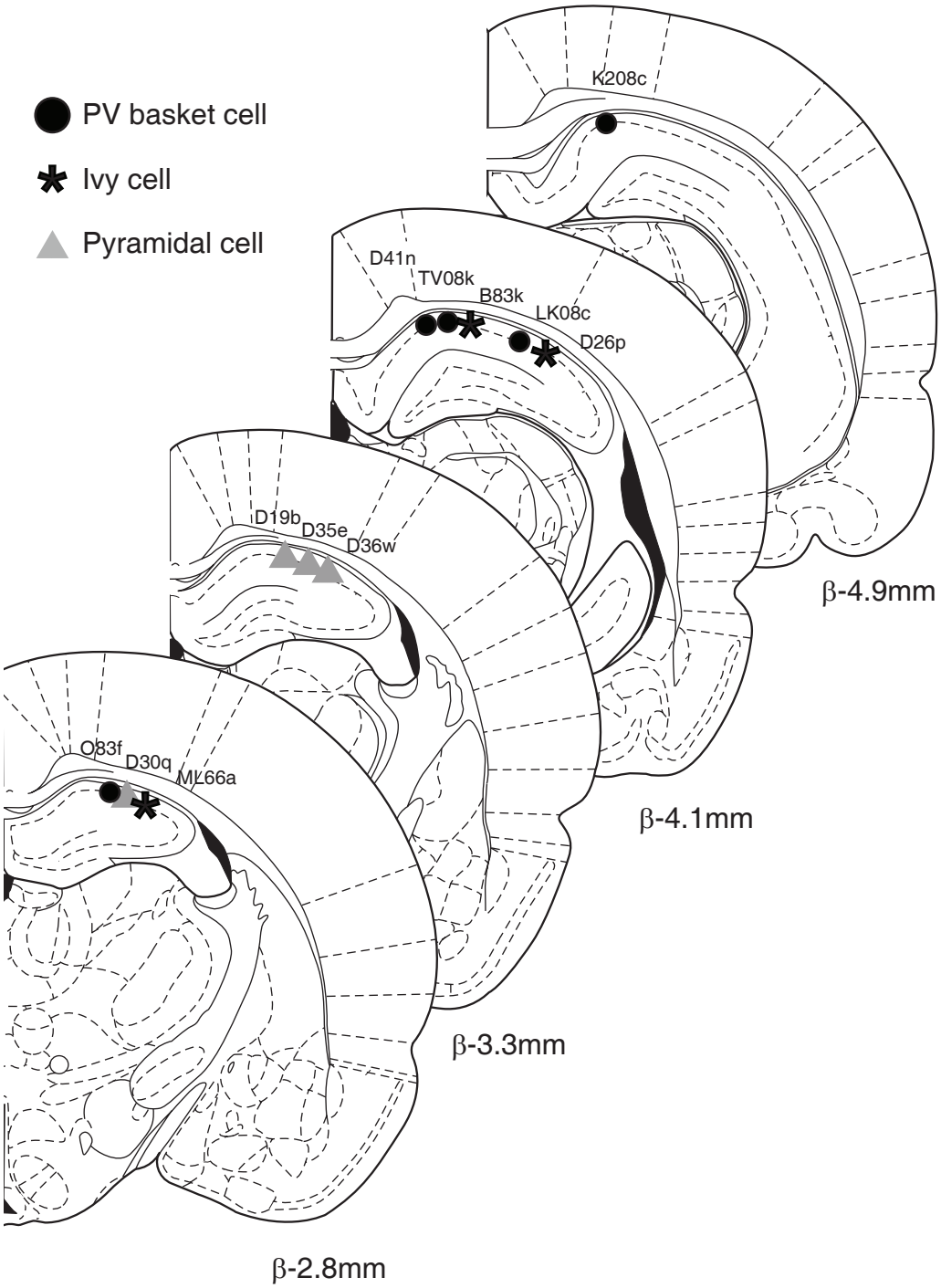

Supplementary Figure 1. Position of recorded cells.

The positions of the recorded and labeled cells together with their individual codes are plotted in the dorsal hippocampus on schematic coronal sections based on the atlas of Paxinos and Watson, 1998.

Nature Neuroscience: doi:10.1038/nn.3176

Supplementary Table 1. List of primary antibodies

molecule	host animal	internal ref number	dilution	source	source code	epitope, amino acid residues	stock protein concentration	specificity reference
calbindin	rabbit	989	1:5000	Swant, Bellinzona, Switzerland	CB-38	raised against recombinant rat calbindin D-28k.	unknown	Airaksinen, M.S., et al. *Proc. Natl. Acad. Sci.* 94, 1488 (1997) - KO test
CCK	guinea pig	1306	1:500, 1:1000	Dr. M. Watanabe, Hokkaido University, Japan	CCK-8	cysteine-taged CCK-8 (CDYMGWMDF) coupled to keyhole limpet hemocyanin	affinity purfied 380µg/ml	labeling pattern as published with other antibodies
	rabbit	1090	1:500	Dr. M. Watanabe, Hokkaido University, Japan	pro-CCK	cysteine-taged C-terminal 9 aa of pro-CCK (CSAEDYEYPS) coupled to keyhole limpet hemocyanin	affinity purfied 350µg/ml	labeling pattern as published with other antibodies
GABAAR α1 subunit	guinea pig	1380	1:200	Prof. R. Shigemoto, Div. Cerebral Structure, Nat. Inst. Physiological Sciences, Okazaki, Japan. Purified by Prof W. Sieghart, Brain Res. Inst., Vienna, Austria.	-	fusion protein, mouse α1 subunit, aa 328-382	affinity purified antibody	Kaufmann, W.A., et al. *J. Comp. Neurol.* 515, 215 (2009); Western blot - Cell expression test
	rabbit	946	1:500, 1:1500	Prof. W. Sieghart, Brain Res. Inst., Vienna, Austria	P16	rat sequence, 1-9	406µg/ml	Zezula, J. & Sieghart, W. *FEBS Lett.* 284, 15 (1991); Baude, A. et al. *Cereb. Cortex* 17, 2094 (2007) - KO test
	rabbit	1389	1:250	Prof. W. Sieghart, Brain Res. Inst., Vienna, Austria	19-8	rat sequence, 1-9	272µg/ml	Zezula, J. & Sieghart, W. *FEBS Lett.* 284, 15 (1991); Baude, A. et al. *Cereb. Cortex* 17, 2094 (2007).
ErbB4	mouse	1353	1:1000, 1:500, 1:100	Thermo Scientific	MS-270-P0	extracellular fragment of recombinant human c-erbB-4/HER-4 oncoprotein	200µg/ml	Neddens, J., et al. *Biol. Psychiatry* 70, 636 (2011); Vullhorst, D., et al. *J. Neurosci.* 29, 12255 (2009); Chen, X., et al. *J. Biol. Chem.* 271, 7620 (1996) - KO test
GABAAR δ subunit	rabbit	912	1:250	Prof. W. Sieghart, Brain Res. Inst., Vienna, Austria	-	rat sequence, aa 1-44	449µg/ml	Jones, A., et al. *J. Neurosci.* 17, 1350 (1997); Tretter, V., et al. *J. Biol. Chem.* 276, 10532 (2001) - KO test
	rabbit	913	1:250	Prof. W. Sieghart, Brain Res. Inst., Vienna, Austria	-	rat sequence, aa 1-44	563µg/ml	Jones, A., et al. *J. Neurosci.* 17, 1350 (1997); Tretter, V., et al. *J. Biol. Chem.* 276, 10532 (2001) - KO test
	rabbit	1342	1:1000	Prof. W. Sieghart, Brain Res. Inst., Vienna, Austria	-	mixture of two affinity purified antidbodies, rat sequences, aa 1-44 and aa 318-400	unknown	Jones, A., et al. *J. Neurosci.* 17, 1350 (1997).
NK1R	guinea pig	991	1:250	Millipore, Chemicon, Temecula, CA, USA	AB5800	synthetic peptide, amino acids 393-407 from rat Substance P Receptor	unknown	Le Brun, I., et al. *Neurosci.* 152, 56 (2008).
	rabbit	1301	1:500, 1:1000	Millipore, Chemicon, Temecula, CA, USA	AB5060	synthetic peptide that corresponds to a 23 amino acid sequence (385-407) of the COOH terminus of the rat Substance P receptor (NK-1)	unknown	labeling pattern as published with other antibodies - Baker, S.J., et al. *Brain. Res. Mol. Brain. Res.* 111, 136 (2003).
nNOS	mouse	1167	1:500, 1:1000	Sigma	N2280 Lot 081K4815	raised to recombinant rat nNOS residues 1-181.	ascites, 35.9 mg/ml	labeling pattern as published with other antibodies
NPY	rabbit	587	1:5000	Peptide Institute, Osaka, Japan	14158-v Lot 864-410804	NPY (human) - bovine thyroglobuline	full serum	RIA-tesed against several neuropeptides
	rabbit	1011	1:5000	Diasorin (Immunostar)	Cat No:-22940	NPY coupled to bovine thyroglobulin (with glutaraldehyde)	unknown	labeling pattern as published with other antibodies; absorption tested by manufacturer to 6 other peptides, leaving reactivity intact.
PV	goat	1258	1:1000	Swant, Bellinzona, Switzerland	PVG-214 Lot 3.6	purified rat PV	unknown	characterized by western blot on rodent brain homogenate and labels a single band at ~12kDa (E. Celio, personal communication) (from Constantinople et al., *J. Comp. Neurol.* 516, 291 (2009)
	guinea pig	1310	1:2000, 1:5000	SYSY Synaptic Systems	195 004	recombinant full length rat parvalbumin	unknown	labeling pattern as published with previous antibodies.
	mouse	922	1:5000	Swant, Bellinzona, Switzerland	235 Lot 10-11 (F)	purified carp PV	unknown	Celio, M.R., et al. *Cell. Calcium* 9, 81 (1988).
	rabbit	835	1:500	Swant, Bellinzona, Switzerland	PV-28 Lot 5.5	purified rat PV	unknown	Kagi, U., et al. *J. Biol. Chem.* 262, 7314 (1987); Schwaller, B., et al. *Am. J. Physiol.* 276, C395 (1999) - KO test
reelin	mouse	1112	1:1000	Chemicon	MAB5364 Lot LV1566698	recombinant reelin amino acids 164-496	1mg/ml	de Bergeyck, V., et al. *J. Neurosci. Methods* 82, 17 (1998).
SATB1/2	mouse	1341	1:100	Abcam	ab51502	recombinant fragment C-terminal (human)	0.1mg/ml	Britanova, O., et al. *Neuron* 57, 378 (2008); Britanova, O., et al. *Eur. J. Neurosci.* 21, 658 (2005); Nielsen, J.V., et al. *Cereb. Cortex* 20, 1904 (2010).
somatostatin	mouse	1276	1:200, 1:500	GeneTex Incorporate	GTX71935 cloneSOM-018	monoclonal, somatostatin conjugated to protein carrier	0.14mg/ml	labeling pattern as published with other antibodies
	rat	815	1:500	Chemicon	MAB354	monoclonal, synthetic 1-14 cyclic somatostatin conjugated to bovine thyroglobulin using carbodiimide	1mg/ml	labeling pattern as published with previous antibodies - Kubota, Y., et al. *Cereb. Cortex* 21, 1803 (2011).
VIP	mouse	1053	1:50000	Dr. G. Ohning, Cure, UCLA, USA	55	monoclonal, raised in mouse against VIP	unknown	Wong, H.C., et al. *Hybridoma* 15, 133 (1996).

Nature Neuroscience: doi:10.1038/nn.3176